

W physics at the LHC with FEWZ 2.1

Ryan Gavin¹, Ye Li^{2,3}, Frank Petriello^{2,3}, and Seth Quackenbush³

¹*Paul Scherrer Institut, CH-5232 Villigen PSI, Switzerland*

²*Department of Physics & Astronomy, Northwestern University, Evanston, IL 60208, USA*

³*High Energy Physics Division, Argonne National Laboratory, Argonne, IL 60439, USA*

Abstract

We present an updated version of the FEWZ (**F**ully **E**xclusive **W** and **Z** production) code for the calculation of W^\pm and γ^*/Z production at next-to-next-to-leading order in the strong coupling. Several new features and observables are introduced, and an order-of-magnitude speed improvement over the performance of FEWZ 2.0 is demonstrated. New phenomenological results for W^\pm production and comparisons with LHC data are presented, and used to illustrate the range of physics studies possible with the features of FEWZ 2.1. We demonstrate with an example the importance of directly comparing fiducial-region measurements with theoretical predictions, rather than first extrapolating them to the full phase space.

1 Introduction

Production of W bosons plays several important roles in hadron-collider physics studies. At the Tevatron, this channel furnishes the single most precise measurement of the W -boson mass. The determination of the charge asymmetry between W^+ and W^- production at both the Tevatron and the Large Hadron Collider (LHC) provides important constraints on quark and anti-quark parton distribution functions (PDFs). High-energy production of W bosons acts as a background to searches for the new W' bosons expected in many gauge extensions of the Standard Model, while production of the W in association with jets is a major background to searches for supersymmetry and other theories beyond the Standard Model with missing-energy signatures. Production of W bosons is copious at the LHC, and the statistical errors have already been rendered completely negligible with the few inverse femtobarns of data taken. Only systematic errors remain, arising from both experimental and theoretical sources. In many of the relevant observables, the experimental systematic errors are already at the few-percent level or smaller.

The theoretical understanding of W production has reached an advanced stage. The inclusive $O(\alpha_S^2)$ QCD corrections to electroweak gauge boson production have been known for some time [1]. Exclusive production, which is necessary for any realistic prediction or phenomenological study in a detector of finite acceptance, is technically challenging but has been achieved [2, 3, 4, 5, 6, 7]. The electroweak and QED corrections are known [8, 9], including the leading-logarithmic terms arising from multiple-photon emission [10]. Initial efforts toward the combination of higher-order QCD and electroweak corrections have been made [11, 12, 13], and even progress toward the exact mixed QED-QCD [14] and next-to-next-to-leading order QED corrections [15] has occurred. The remaining theoretical uncertainties are estimated to be at the percent level for the majority of relevant observables. These corrections are available to the experimental community in a variety of simulation codes.

We have previously released a 2.0 version of the simulation code FEWZ (**F**ully **E**xclusive **W** and **Z** Production) that implements the NNLO QCD predictions for neutral-current γ^*/Z production at hadron colliders, and allows for arbitrary kinematic cuts to be imposed [16]. FEWZ features a parallelized integration routine suited for running on modern computer clusters, allows for multiple, arbitrary kinematic variables to be binned during a single run, and automatically calculates PDF errors for the total cross section and all histogram bins. It has been used by collaborations at the Tevatron, the LHC, and RHIC in their physics studies. The purpose of this work is to apply the advances in FEWZ 2.0 to the description of W production also, and to introduce further improvements to the FEWZ framework, resulting in a FEWZ 2.1 version. We have further improved the integration routine to provide an additional order-of-magnitude gain in speed. FEWZ 2.1 incorporates the LHAPDF format [17] to allow all PDF sets of interest to be studied. Several new observables are introduced in the new version of the program.

Our manuscript is organized as follows. We discuss the new features of FEWZ 2.1 in Section 2. Both the new available observables and the performance increase are detailed. In Section 3 we present phenomenological results for W physics at the LHC. We present compar-

isons of both integrated cross sections within the fiducial region and the charge asymmetry with ATLAS data. Several ratios of W^+ over W^- distributions are shown, both to illustrate the range of studies possible with the scripts distributed with FEWZ 2.1, and to highlight physics features of W production at the LHC. The importance of directly comparing fiducial-region measurements to theoretical predictions, rather than first extrapolating them to the full phase space, is demonstrated using the W^+ over W^- cross section ratio. Only before the extrapolation is the measurement error small enough to allow for discrimination between different PDF sets. We conclude in Section 4.

2 New features

Version 2.1 applies all improvements of FEWZ 2.0 [16] to W boson production. The user may now make either of two executables, `fewzw` or `fewzz`, which correspond to W or γ^*/Z production, respectively. Most source code is shared between the two executables. The sector structure is slightly different owing to a few differing diagrams and symmetry factors at NNLO between W and γ^*/Z production. Both executables take similar basic input files, and the same histogram input. The user of FEWZ 2.0 will not notice significant differences in compiling and running the new version of the program. We highlight below several new features of FEWZ 2.1.

2.1 New observables

We have added two new observables to further facilitate physics studies.

- Beam thrust [18] has been added as an available histogram in FEWZ 2.1. Beam thrust is defined in FEWZ 2.1 as a sum over observed jets [19]:

$$\tau_B = \frac{1}{Q} \sum_k |\vec{p}_{k,T}| e^{-|\eta_k - Y|}, \quad (1)$$

where Q and Y are the dilepton invariant mass and rapidity, and $\vec{p}_{k,T}$ and η_k refer to the transverse momentum and pseudorapidity of the k -th jet. Beam thrust permits a central jet veto to be imposed without a jet algorithm, making it more easily amenable to resummation techniques. We include it to facilitate comparison between fixed-order results and resummation results, as well as for study in its own right.

- The transverse mass has been added to allow for W production studies. Transverse mass is defined as

$$M_T = \sqrt{2p_{Tl}E_{Tmiss}(1 - \cos(\Delta\phi_{l,miss}))}. \quad (2)$$

p_{Tl} refers to the transverse momentum of the charged lepton, E_{Tmiss} refers to the transverse momentum of the neutrino, and $\Delta\phi_{l,miss}$ denotes the angular separation

between them in the transverse plane. M_T has a Jacobian peak sensitive to the mass of the W without being dependent on the unobserved longitudinal momentum of the neutrino. It is defined analogously for the Z for comparison purposes.

Both new observables are available for creating histograms; cuts on transverse mass are also accessible in the input file.

2.2 New output features

Several new possibilities for controlling the histogram output have been added.

- The user now has the option to output cumulative histograms in addition to traditional ones. This can be useful to study the effect of cut placement on the variable of interest. This feature adds more than the convenience of avoiding adding histogram bins by hand: the resulting technical precision on a cumulative bin is better due to cancellations between bins.
- Most experimental analyses use bin sizes that vary over the range of the histogram. Formerly this could be handled in FEWZ at the cost of multiple runs, but now the user has the option to input their own histogram bounds for any given histogram.
- In addition to the scripts of FEWZ 2.0 which allow one to perform addition and multiplication operations on the output of separate runs, an asymmetry operator has been added which directly combines the results of W^+ and W^- runs in the following way:

$$A_W = \frac{\sigma_{W^+} - \sigma_{W^-}}{\sigma_{W^+} + \sigma_{W^-}} \quad (3)$$

Both the statistical and PDF errors are propagated consistently.

2.3 Speed improvements

The sector combinations detailed in [16] have been reworked to provide a modest reduction in variance of the integrand, reducing the time required to reach the target precision. Some of these sectors have undergone “sector recomposition,” which patches together the pieces resulting from sector decomposition [20, 21] by undoing the variable transformations needed in the case of singularities in multiple endpoints of the phase-space integrals. This results in a more consistent mapping of the integration variables to parton phase space for similar sectors. There are now 133 sectors for `fewzz` and 154 for `fewzw`. Alternative techniques for reducing the number of required integrals when applying sector decomposition have been discussed in Ref. [22]. We have also been careful to eliminate redundancies caused by calling the same code with the same arguments repeatedly. Instead, the results of these calls (where they cannot be avoided) are stored in a cache or buffer. Finally, we have rearranged how certain variables are stored, so that access is more likely to occur contiguously in memory, resulting

in fewer CPU cache misses. This can make a large difference in the case of parton distribution functions, which are accessed frequently, or histograms, which are filled frequently.

Altogether, the speed improvements are significant. In Fig. 1, we reproduce Fig. 1 of [16], which shows integration precision as a function of time. FEWZ 2.1 has been added to the comparison. The cuts, histograms, PDF sets, and benchmark machine are the same as Ref. [16], with the exception of the addition of the two new histograms described in Sec. 2.2. The time required to reach a target precision is an order of magnitude less than needed for FEWZ 2.0.

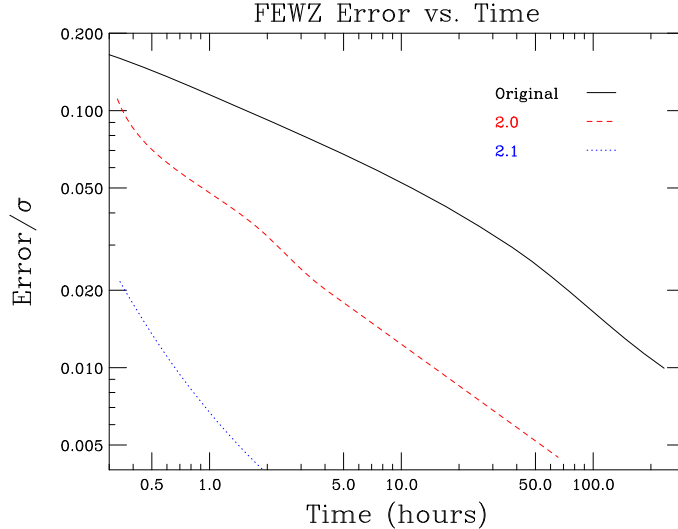


Figure 1: Relative error versus time for different versions of FEWZ.

3 Example results

To demonstrate the capabilities of FEWZ 2.1, we present in this section several results relevant for the study of W -boson production at the LHC. We impose the following set of standard acceptance cuts on the W -decay products:

$$\begin{aligned} M_T &> 40 \text{ GeV}, & E_{T_{miss}} &> 25 \text{ GeV}, \\ p_{Tl} &> 20 \text{ GeV}, & |\eta_l| &< 2.5. \end{aligned} \tag{4}$$

We begin by studying the total cross section for W^\pm production subject to these cuts, together with the ratio of W^+ over W^- within this phase-space region. To illustrate the sensitivity of the cross section to different extractions of parton distribution functions, we show results for three NNLO PDF fits: those of HERA [23], MSTW [24], and NNPDF [25] (to avoid clutter in the plots and tables we do not show the NNLO results of ABKM [26] or

JR [27], which have been presented in our previous work on Z physics [16]).

$$\begin{aligned}
\text{HERA:} \quad & \sigma_{W^-} = 2134_{-22}^{+15} \text{ pb}; \quad \sigma_{W^+} = 3265_{-31}^{+37} \text{ pb}; \quad \frac{\sigma_{W^+}}{\sigma_{W^-}} = 1.530_{-0.015}^{+0.017} \\
\text{MSTW:} \quad & \sigma_{W^-} = 2106_{-35}^{+35} \text{ pb}; \quad \sigma_{W^+} = 3181_{-55}^{+57} \text{ pb}; \quad \frac{\sigma_{W^+}}{\sigma_{W^-}} = 1.510_{-0.013}^{+0.014} \\
\text{NNPDF:} \quad & \sigma_{W^-} = 2085_{-32}^{+32} \text{ pb}; \quad \sigma_{W^+} = 3255_{-52}^{+52} \text{ pb}; \quad \frac{\sigma_{W^+}}{\sigma_{W^-}} = 1.563_{-0.026}^{+0.026}.
\end{aligned} \tag{5}$$

The 68% C.L. PDF errors are shown for each set. The parametric uncertainties arising from imprecise knowledge of the strong coupling and other parameters are not included in these results. Scale uncertainties have previously been shown to be subdominant to PDF uncertainties for electroweak gauge boson production at the LHC [16, 30]. We note that the technical errors arising from the integration error are less than 0.1%. The results for each PDF set are consistent, although the MSTW results for σ_{W^+} and the ratio are more than one sigma lower than the results for the other sets. We compare the results above with the ATLAS results for the $\sigma_{W^+}/\sigma_{W^-}$ ratio [28]:

$$\left(\frac{\sigma_{W^+}}{\sigma_{W^-}} \right)_{\text{fid}} = 1.542 \pm 0.007(\text{stat.}) \pm 0.012(\text{sys.}) \pm 0.001(\text{accept.}). \tag{6}$$

We note that ATLAS combines both the electron and muon channels and extrapolates them to a common fiducial region when obtaining this number. The subscript 'fid.' denotes that the ratio is measured in this common region, which coincides exactly with the phase space defined by our standard acceptance cuts. The last error labeled accept. denotes the uncertainty contribution arising from extrapolation. The NNPDF and HERA PDF predictions are consistent within one sigma from the ATLAS measurement, while the MSTW result differs by over two sigma from the central value of the measurement. The situation becomes murkier if the ratio of inclusive cross sections is compared instead. In that case, the measured fiducial cross section is extrapolated to the full phase space using Monte Carlo simulation, introducing an additional source of uncertainty. The ATLAS measurement of the inclusive ratio is

$$\left(\frac{\sigma_{W^+}}{\sigma_{W^-}} \right)_{\text{inc}} = 1.454 \pm 0.006(\text{stat.}) \pm 0.012(\text{sys.}) \pm 0.022(\text{accept.}). \tag{7}$$

Upon combining the various sources of uncertainty in quadrature, an error twice as large as the one in Eq. (6) is obtained. This result should be compared with the theoretical predictions for the inclusive cross section ratio:

$$\begin{aligned}
\text{HERA :} \quad & (\sigma_{W^+}/\sigma_{W^-})_{\text{inc}} = 1.440_{-0.014}^{+0.015}, \\
\text{NNPDF :} \quad & (\sigma_{W^+}/\sigma_{W^-})_{\text{inc}} = 1.471_{-0.020}^{+0.020}, \\
\text{MSTW :} \quad & (\sigma_{W^+}/\sigma_{W^-})_{\text{inc}} = 1.435_{-0.010}^{+0.013}.
\end{aligned} \tag{8}$$

All three sets now agree within the estimated one-sigma uncertainty with the results in Eq. (7). The full potential of the experimental measurement to distinguish between different

PDF extractions is only realized if the fiducial cross sections can be directly compared to theoretical predictions. With FEWZ 2.1, this becomes possible. We note that a comparison of CMS results [29] with the W^+ over W^- inclusive cross section ratio obtained with different NNLO PDF sets was presented in Ref. [30], where a similar point regarding the importance of studying the fiducial cross sections was made. In that study, parametric uncertainties on the ratio of W^+ over W^- cross sections were also studied, and found to increase the PDF-only error by a negligible amount. We rely on this result to safely neglect them here.

We next present results for several distributions, to illustrate both the functioning of FEWZ 2.1 and aspects of W physics at the LHC. The transverse mass and rapidity distributions for W^\pm are shown in Fig. 2. The Jacobian peaks for $M_T = M_W$ are clearly seen in both plots. Also visible is a similar, although less prominent, feature at $M_T = 50$ GeV caused by the cuts of Eq. (4). At leading order, the missing E_T and the lepton momentum must be equal and back-to-back in the transverse plane, leading to the noted minimum. This constraint is relaxed at higher orders when the W^\pm can recoil against additional radiation, populating the region $40 \text{ GeV} < M_T < 50 \text{ GeV}$. The stronger peaking of the up-quark PDF as compared to the down-quark distribution at $x \sim 0.1$ is visible in the enhancement of the W^+ rapidity distribution near $|Y| \sim 2$.

In order to illustrate new features present in FEWZ 2.1, we present in Fig. 3 results for the W^- beam thrust and the W^+ cumulative leading-jet p_T distributions. No significant distributions between the three PDF sets are found for either observable. Additional radiation in W production goes like $C_F\alpha_s/\pi$. This is a smaller quantity than the $C_A\alpha_s/\pi$ relevant for gluon-initiated processes, and explains the peaking of the beam-thrust distribution at lower values than observed in Ref. [31] for Higgs production and the quick plateau observed in the leading-jet transverse momentum distribution.

The scripts distributed with FEWZ allow ratios of kinematic distributions to be easily studied by combining the results of separate runs. We present below in Fig. 4 several examples relevant to LHC phenomenology. The ratio W^+ over W^- production as a function of both lepton pseudorapidity and transverse momentum is shown in Fig. 4 for the MSTW, NNPDF, and HERAPDF PDF sets. In the left panel, a separation between the sets is apparent at central rapidity, larger than the estimated PDF uncertainty. The ratio of lepton p_T distributions shown in the right panel reveals a harder distribution for the W^- than the W^+ . This can be understood by considering the leading-order kinematics. The p_T and η of the lepton can be written in terms of the center-of-momentum frame scattering angle as $p_T = \sqrt{\hat{s}} \sin \theta / 2$, $\eta = -\ln \tan(\theta/2)$. The larger fraction of events at large rapidity for W^+ observed in Fig. 2 translates into a larger fraction of events at larger lepton pseudorapidity for W^+ than for W^- . The leading-order kinematics implies that W^+ events with large η have scattering angles with small $\sin \theta$, and consequently smaller lepton p_T than those for W^- production.

The W charge asymmetry as a function of lepton pseudorapidity, defined as

$$\frac{dA_W}{d\eta_l} = \frac{d\sigma_{W^+}/d\eta_l - d\sigma_{W^-}/d\eta_l}{d\sigma_{W^+}/d\eta_l + d\sigma_{W^-}/d\eta_l} \quad (9)$$

is well-known to provide a strong constraint on PDFs. We compare in Fig. 5 the bin-

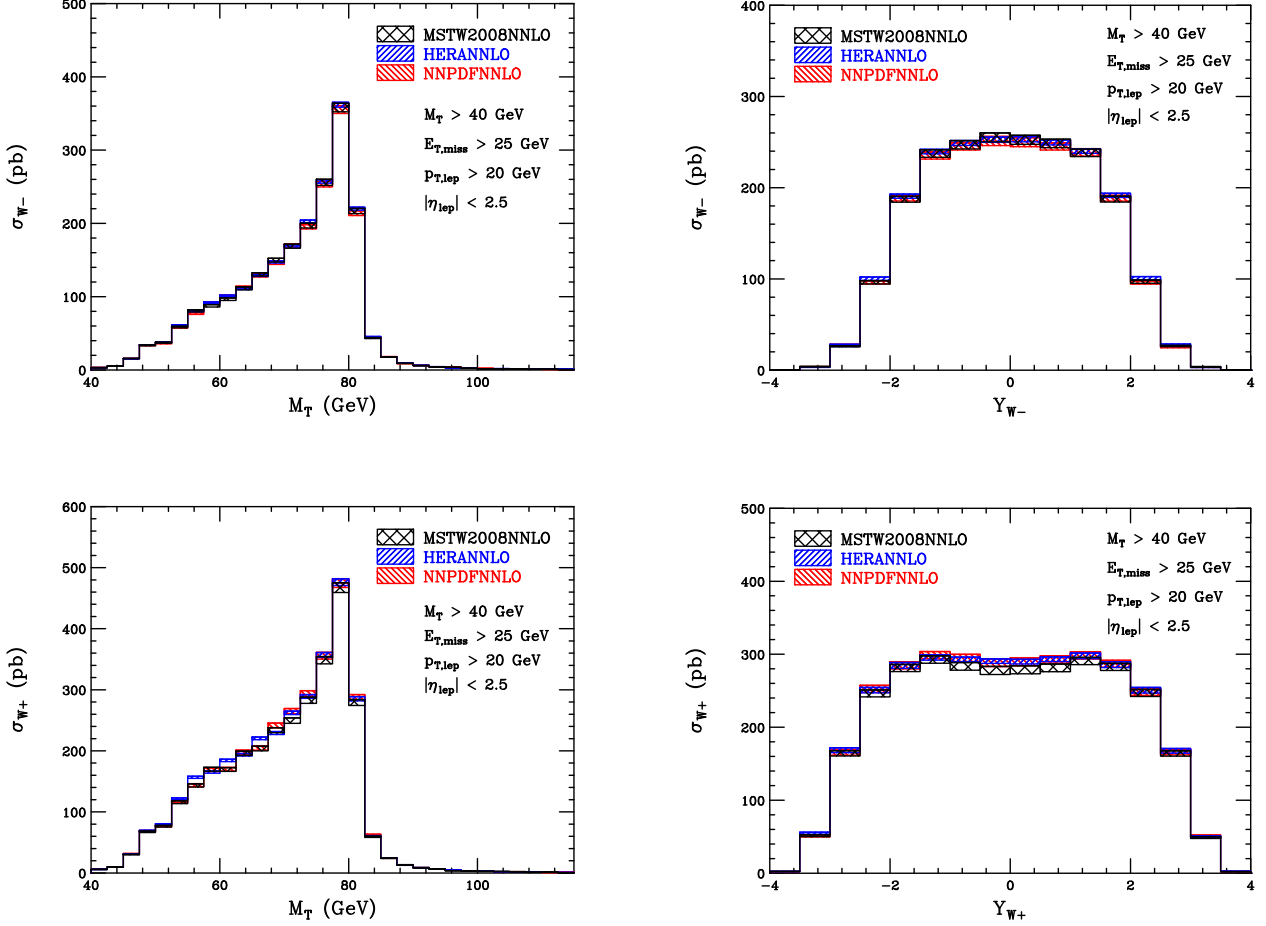


Figure 2: Bin-integrated cross sections for the W^- transverse mass (upper left panel), W^- rapidity (upper right panel), W^+ transverse mass (lower left panel), and W^+ rapidity (lower right panel) for all three NNLO PDF sets. The standard acceptance cuts of Eq. (4) have been implemented. The bands indicate the PDF uncertainties for each set.

integrated results for A_W for the MSTW, NNPDF, and HERAPDF sets with recent results from ATLAS [28]. The HERAPDF and NNPDF predictions are in good agreement with the data over the experimentally available range of pseudorapidity, while the MSTW predictions are slightly lower throughout this range.

4 Conclusions

We have presented an update to the program FEWZ, version 2.1, which extends the functionality of FEWZ 2.0 to allow for the study of W physics at hadron colliders. Several new features have been added, including new observables, the possibility of cumulative histograms or ones with varying bin sizes, and an interface to the PDF library LHAPDF. Major speed improvements have been achieved; NNLO precision in the presence of standard acceptance

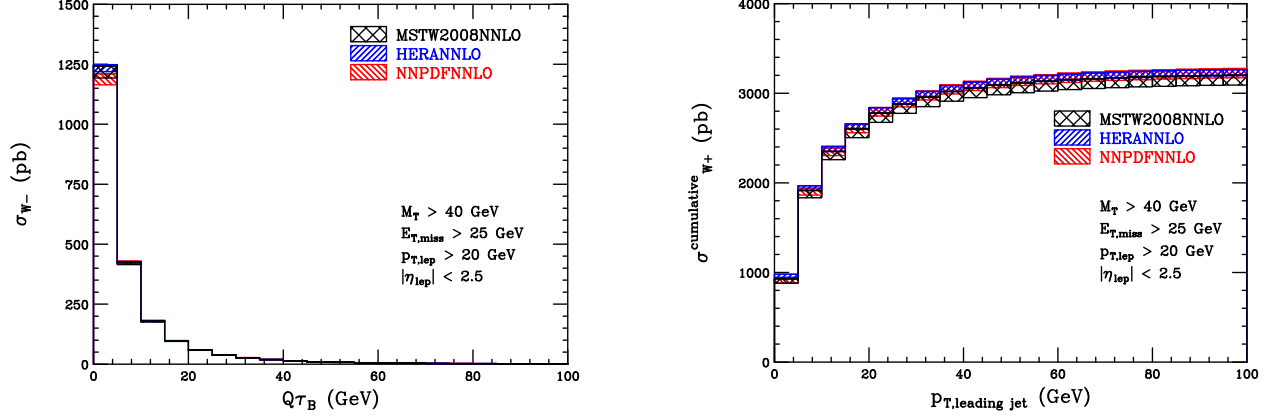


Figure 3: Bin-integrated cross sections for the W^- beam-thrust distribution (left panel) and the cumulative leading-jet p_T distribution in W^+ production (right panel).

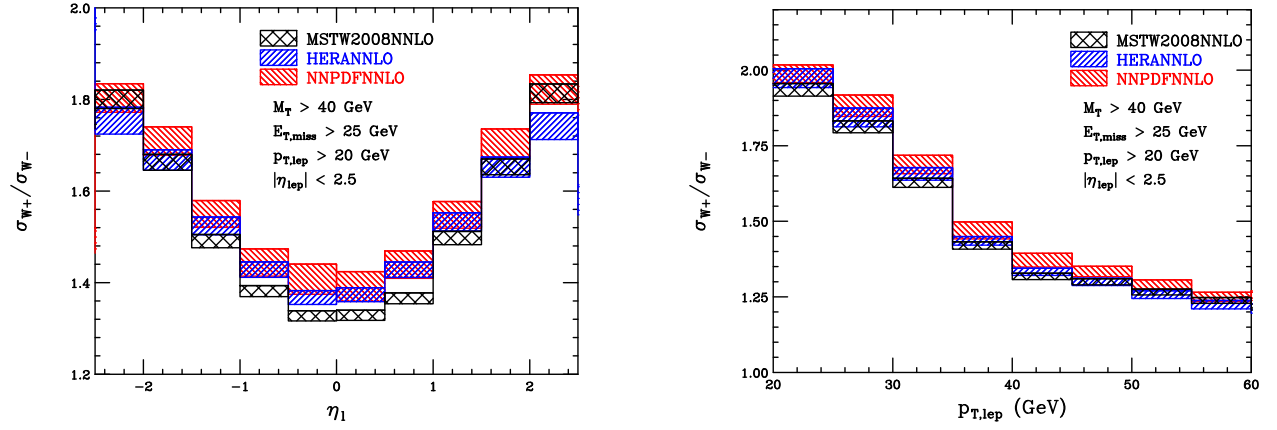


Figure 4: Ratio of W^+ over W^- production as a function of lepton pseudorapidity (left panel), and lepton p_T (right panel).

cuts can now be achieved on a single machine in hours. We have presented example runs of the new code for W observables with several NNLO PDF sets, both to show aspects of W physics at the LHC and to demonstrate the array of studies possible with the analysis scripts distributed with FEWZ 2.1. Comparisons to early LHC data indicate excellent agreement of data and theory as calculated by FEWZ. With FEWZ, the extrapolation of measured quantities to the full phase space and consequent increase in experimental uncertainty can be avoided. We look forward to the continued use of FEWZ in understanding the properties of electroweak gauge bosons at hadron colliders with unprecedented accuracy.

Acknowledgements

We thank U. Klein for considerable input and testing during the initial stages of integrating the W code, and K. Mueller, W. Sakumoto, S. Stoynev, and H. Yoo for substantial helpful

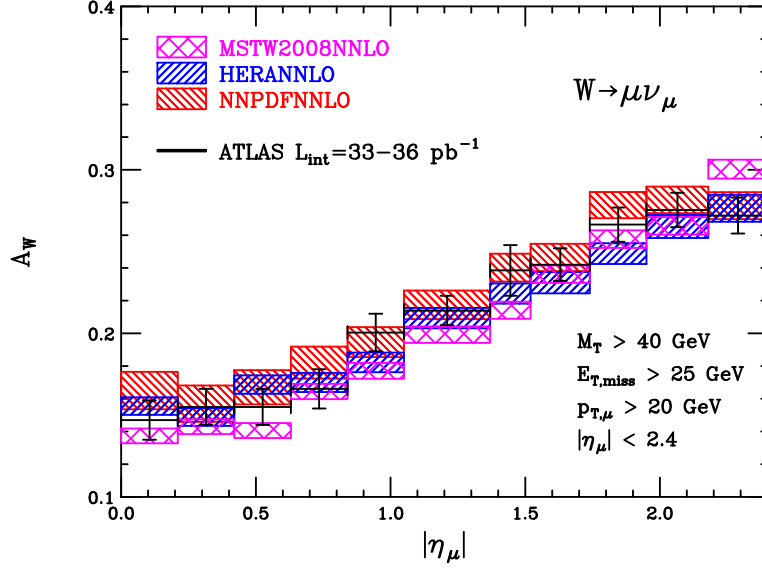


Figure 5: Charge asymmetry at NNLO for three different PDF sets, compared with recent data from ATLAS.

feedback. This research is supported by the US DOE under contract DE-AC02-06CH11357 and the grant DE-FG02-91ER40684, and by the Swiss National Science Foundation.

References

- [1] R. Hamberg, W. L. van Neerven and T. Matsuura, Nucl. Phys. B **359**, 343 (1991) [Erratum-ibid. B **644**, 403 (2002)].
- [2] C. Anastasiou, L. J. Dixon, K. Melnikov and F. Petriello, Phys. Rev. Lett. **91**, 182002 (2003) [hep-ph/0306192].
- [3] C. Anastasiou, L. J. Dixon, K. Melnikov and F. Petriello, Phys. Rev. **D69**, 094008 (2004) [hep-ph/0312266].
- [4] K. Melnikov and F. Petriello, Phys. Rev. Lett. **96**, 231803 (2006) [arXiv:hep-ph/0603182].
- [5] K. Melnikov and F. Petriello, Phys. Rev. D **74**, 114017 (2006) [arXiv:hep-ph/0609070].
- [6] S. Catani, L. Cieri, G. Ferrera, D. de Florian and M. Grazzini, Phys. Rev. Lett. **103**, 082001 (2009) [arXiv:0903.2120 [hep-ph]].
- [7] S. Catani, G. Ferrera and M. Grazzini, JHEP **1005**, 006 (2010) [arXiv:1002.3115 [hep-ph]].

- [8] U. Baur, S. Keller and D. Wackerth, Phys. Rev. D **59**, 013002 (1999) [hep-ph/9807417].
- [9] S. Dittmaier and M. Kramer, Phys. Rev. D **65**, 073007 (2002) [hep-ph/0109062].
- [10] C. M. Carloni Calame, G. Montagna, O. Nicrosini and A. Vicini, JHEP **0612**, 016 (2006) [hep-ph/0609170].
- [11] Q. -H. Cao and C. P. Yuan, Phys. Rev. Lett. **93**, 042001 (2004) [hep-ph/0401026].
- [12] G. Balossini, G. Montagna, C. M. Carloni Calame, M. Moretti, O. Nicrosini, F. Piccinini, M. Treccani and A. Vicini, JHEP **1001**, 013 (2010) [arXiv:0907.0276 [hep-ph]].
- [13] C. Bernaciak and D. Wackerth, arXiv:1201.4804 [hep-ph].
- [14] W. B. Kilgore and C. Sturm, arXiv:1107.4798 [hep-ph].
- [15] R. Boughezal, K. Melnikov and F. Petriello, arXiv:1111.7041 [hep-ph].
- [16] R. Gavin, Y. Li, F. Petriello and S. Quackenbush, Comput. Phys. Commun. **182**, 2388 (2011) [arXiv:1011.3540 [hep-ph]].
- [17] M. R. Whalley, D. Bourilkov and R. C. Group, arXiv:hep-ph/0508110.
- [18] I. W. Stewart, F. J. Tackmann and W. J. Waalewijn, Phys. Rev. D **81**, 094035 (2010) [arXiv:0910.0467 [hep-ph]].
- [19] I. W. Stewart, F. J. Tackmann and W. J. Waalewijn, Phys. Rev. Lett. **106**, 032001 (2011) [arXiv:1005.4060 [hep-ph]].
- [20] C. Anastasiou, K. Melnikov and F. Petriello, Phys. Rev. D **69**, 076010 (2004) [hep-ph/0311311].
- [21] C. Anastasiou, K. Melnikov and F. Petriello, Nucl. Phys. B **724**, 197 (2005) [hep-ph/0501130].
- [22] C. Anastasiou, F. Herzog and A. Lazopoulos, JHEP **1103**, 038 (2011) [arXiv:1011.4867 [hep-ph]].
- [23] A. M. Cooper-Sarkar [ZEUS and H1 Collaborations], arXiv:1112.2107 [hep-ph].
- [24] A. D. Martin, W. J. Stirling, R. S. Thorne and G. Watt, Eur. Phys. J. C **63**, 189 (2009) [arXiv:0901.0002 [hep-ph]].
- [25] R. D. Ball *et al.* [The NNPDF Collaboration], Nucl. Phys. B **855**, 153 (2012) [arXiv:1107.2652 [hep-ph]].
- [26] S. Alekhin, J. Blumlein, S. Klein and S. Moch, arXiv:0908.3128 [hep-ph].

- [27] P. Jimenez-Delgado and E. Reya, Phys. Rev. D **80**, 114011 (2009) [arXiv:0909.1711 [hep-ph]].
- [28] G. Aad *et al.* [ATLAS Collaboration], arXiv:1109.5141 [hep-ex].
- [29] S. Chatrchyan *et al.* [CMS Collaboration], JHEP **1110**, 132 (2011) [arXiv:1107.4789 [hep-ex]].
- [30] G. Watt, JHEP **1109**, 069 (2011) [arXiv:1106.5788 [hep-ph]].
- [31] C. F. Berger, C. Marcantonini, I. W. Stewart, F. J. Tackmann and W. J. Waalewijn, JHEP **1104**, 092 (2011) [arXiv:1012.4480 [hep-ph]].